

CrossMark  
click for updatesCite this: *Catal. Sci. Technol.*, 2016,  
6, 288

## Molecular determinants for selective C<sub>25</sub>-hydroxylation of vitamins D<sub>2</sub> and D<sub>3</sub> by fungal peroxxygenases†

Fátima Lucas,<sup>‡\*a</sup> Esteban D. Babot,<sup>‡b</sup> Marina Cañellas,<sup>‡ac</sup> José C. del Río,<sup>b</sup>  
Lisbeth Kalum,<sup>d</sup> René Ullrich,<sup>e</sup> Martin Hofrichter,<sup>e</sup> Victor Guallar,<sup>af</sup>  
Angel T. Martínez<sup>g</sup> and Ana Gutiérrez<sup>\*b</sup>

Hydroxylation of vitamin D by *Agrocybe aegerita* and *Coprinopsis cinerea* peroxxygenases was investigated in a combined experimental and computational study. 25-Monohydroxylated vitamins D<sub>3</sub> (cholecalciferol) and D<sub>2</sub> (ergocalciferol), compounds of high interest in human health and animal feeding, can be obtained through a reaction with both fungal enzymes. Differences in conversion rates, and especially in site selectivity, were observed. To rationalize the results, diffusion of D<sub>2</sub> and D<sub>3</sub> on the molecular structure of the two enzymes was performed using the PELE software. In good agreement with experimental conversion yields, simulations indicate more favorable energy profiles for the substrates' entrance in *C. cinerea* than for *A. aegerita* enzyme. On the other hand, GC-MS analyses show that while a full regioselective conversion of D<sub>2</sub> and D<sub>3</sub> into the active C<sub>25</sub> form is catalyzed by *C. cinerea* peroxxygenase, *A. aegerita* yielded a mixture of the hydroxylated D<sub>3</sub> products. From the molecular simulations, relative distance distributions between the haem compound I oxygen atom and H<sub>24</sub>/H<sub>25</sub> atoms (hydrogens on C<sub>24</sub> and C<sub>25</sub>, respectively) were plotted. Results show large populations for O–H<sub>25</sub> distances below 3 Å for D<sub>2</sub> and D<sub>3</sub> in *C. cinerea* in accordance with the high reactivity observed for this enzyme. In *A. aegerita*, however, cholecalciferol has similar populations (below 3 Å) for O–H<sub>25</sub> and O–H<sub>24</sub>, which can justify the hydroxylation observed in C<sub>24</sub>. In the case of ergocalciferol, due to the bulky methyl group in position C<sub>24</sub>, very few structures are found with O–H<sub>24</sub> distances below 3 Å and thus, as expected, the reaction was only observed at the C<sub>25</sub> position.

Received 20th March 2015,  
Accepted 29th July 2015

DOI: 10.1039/c5cy00427f

www.rsc.org/catalysis

### Introduction

Selective oxygenations of aliphatic compounds are among the most challenging reactions in organic chemistry for the regio- and/or stereospecific synthesis of pharmaceuticals and fine chemicals. Monooxygenases catalyzing such hydroxylation

reactions include cytochrome P450, a family of haem proteins playing a variety of physiological roles but often requiring an auxiliary flavoenzyme (or a flavin-containing module) and a source of reducing power to be activated by O<sub>2</sub> – two facts that limit their biotechnological applicability.

Recently, a new peroxidase type, which shares the active site architecture and reaction mechanism of cytochrome P450, but has the advantage of being activated directly by H<sub>2</sub>O<sub>2</sub>, was isolated from *Agrocybe aegerita*,<sup>45</sup> and later identified in a variety of sequenced basidiomycete genomes including that of *Coprinopsis cinerea*.<sup>13</sup> Due to the above characteristics, these unspecific peroxxygenases (EC 1.11.2.1) have huge biotechnological potential as self-sufficient monooxygenases<sup>9,19</sup> for hydroxylation of both aromatic<sup>2,3,24–27,42–44</sup> and aliphatic compounds.<sup>4,15,33</sup>

The *A. aegerita* enzyme has been the most widely investigated basidiomycete peroxxygenase, but recent studies have shown that the *C. cinerea* enzyme has comparative advantages related to its high conversion yield/selectivity for some hydroxylation reactions and its production as a recombinant protein in an industrial expression host (by Novozymes, Bagsvaerd, Denmark).<sup>5,6</sup>

<sup>a</sup> Joint BSC-CRG-IRB Research Program in Computational Biology, Barcelona Supercomputing Center, Jordi Girona 29, E-08034 Barcelona, Spain.

E-mail: fatima.lucas@bsc.es

<sup>b</sup> Instituto de Recursos Naturales y Agrobiología de Sevilla, CSIC, Reina Mercedes 10, E-41012 Seville, Spain. E-mail: anagu@irnase.csic.es; Fax: +32 954624002; Tel: +32 954624711

<sup>c</sup> Anaxomics Biotech, Balmes 89, E-08008 Barcelona, Spain

<sup>d</sup> Novozymes A/S, Krogshoejvej 36, 2880 Bagsvaerd, Denmark

<sup>e</sup> TU Dresden, Department of Bio- and Environmental Sciences, Markt 23, 02763 Zittau, Germany

<sup>f</sup> ICREA, Passeig Lluís Companys 23, E-08010 Barcelona, Spain

<sup>g</sup> Centro de Investigaciones Biológicas, CSIC, Ramiro de Maeztu 9, E-28040 Madrid, Spain

† Electronic supplementary information (ESI) available: Molecular model for *C. cinerea* peroxxygenase obtained using *A. aegerita*'s crystal structure as the template. See DOI: 10.1039/c5cy00427f

‡ These three authors equally contributed to this work

Hydroxylation of vitamin D for the selective production of its active C<sub>25</sub>-hydroxylated derivatives is one of the reactions where the *C. cinerea* peroxygenase can be of biotechnological use (Fig. 1).<sup>6</sup> Supplementation with 25-hydroxyvitamin D has a positive effect on different human diseases,<sup>11,20,21,28,41</sup> and also raises considerable interest for feeding broiler chickens<sup>14,17,23,32</sup> and other farm animals<sup>40</sup> to reduce skeleton problems caused by rapid growth and reduced mobility. Therefore, the use of peroxygenase in vitamin D hydroxylation represents an attractive alternative to the chemical synthesis.

The goal of the present work is to rationalize the differences observed in cholecalciferol and ergocalciferol's (vitamins D<sub>3</sub> and D<sub>2</sub>, respectively) conversion rates and site selectivity by the *A. aegerita* and *C. cinerea* peroxygenases. The work presented here consists of first, the enzymatic conversion of these compounds by the two peroxygenases under the same reaction conditions, and gas chromatography-mass spectrometry (GC-MS) analyses to identify all reaction products. Then, the energy profiles and binding modes of vitamins D<sub>2</sub> and D<sub>3</sub> were determined by structure-based computational simulations, using the PELE software.<sup>10,12</sup> Finally, differences in site selectivity were investigated through the analysis of the most favorable binding orientations in the active site. Results show that molecular simulations can effectively discriminate experimentally observed differences in conversion rates and site selectivity.

## Results and discussion

### Experimental hydroxylation reactions

The conversion of cholecalciferol and ergocalciferol was experimentally determined for both the *A. aegerita* and *C. cinerea* peroxygenases. In the case of cholecalciferol (0.1 mM), GC-MS analyses of the reaction mixture revealed that

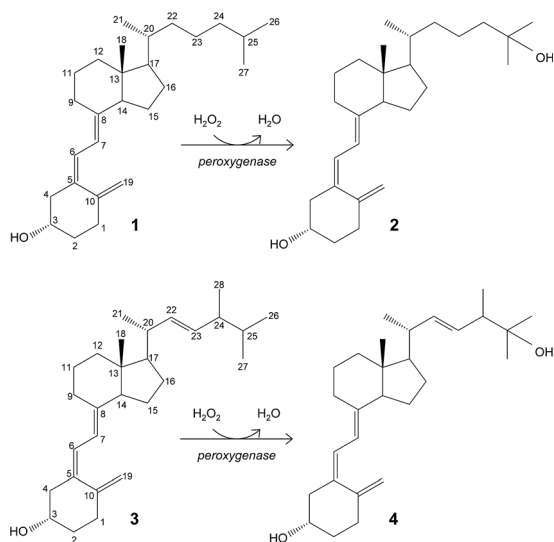


**Fig. 1** Enzymatic conversion of cholecalciferol (vitamin D<sub>3</sub>; **1**) and ergocalciferol (vitamin D<sub>2</sub>; **3**) into their bioactive 25-hydroxylated derivatives (**2** and **4**) by basidiomycete peroxygenases.

this compound was completely (100%) converted by the *C. cinerea* enzyme within 60 min reaction (Fig. 2C) as compared with the control reaction without peroxygenase (Fig. 2A). In the *A. aegerita* peroxygenase reaction, up to 90% conversion was observed (Fig. 2B). In the case of ergocalciferol (Fig. 2D–F), a conversion of 85% was produced by *C. cinerea* while in *A. aegerita* reaction, 81% conversion was observed. When higher substrate concentrations were tested (e.g. 0.5 mM), higher differences in the conversion rates by the two enzymes were observed (40–50% and 20% conversions by the *C. cinerea* and *A. aegerita* peroxygenases, respectively).

Moreover, cholecalciferol and ergocalciferol conversion by the *C. cinerea* peroxygenase showed a strict site selectivity since it gave exclusively 25-hydroxycalciferol. Likewise, conversion by the *A. aegerita* enzyme of ergocalciferol yielded exclusively 25-hydroxyergocalciferol but for cholecalciferol, a mixture of products was observed. The products include 25-hydroxycholecalciferol (64% of the initial substrate) together with 24-hydroxycholecalciferol (21%) and 26/27-hydroxycholecalciferol (7%), as confirmed by comparison with true standards showing identical retention times and mass spectra. The double peaks observed in the chromatograms for both the substrate and the product (Fig. 2) correspond to the isopyro (19β, 9β) and pyro (19α, 9α) isomers formed by a

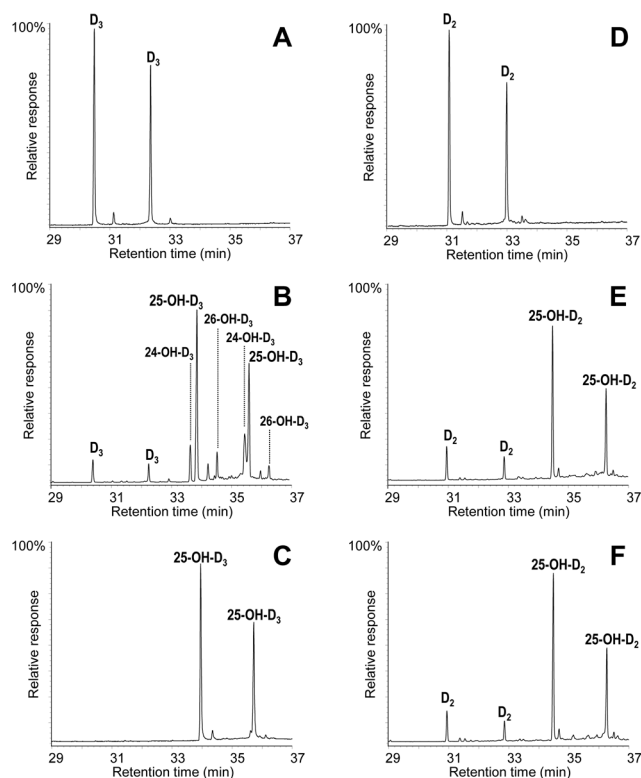


**Fig. 2** GC-MS analyses of cholecalciferol (left) and ergocalciferol (right) hydroxylation by the *A. aegerita* (B, E) and *C. cinerea* peroxygenases (C, F), compared with a control without enzyme showing the substrate peaks (A, D), as TMS derivatives from 60 min reactions. In all cases, the isopyro (left) and pyro (right) isomers from the secosteroid thermal rearrangement are obtained (two small peaks in A and D correspond to minor additional isomers).

thermal rearrangement involving ring-B closure that vitamin D and its hydroxylated derivatives undergo due to the temperature at which GC-MS EI(+) is carried out. Indeed, the presence of the two isomers during GC separation is a useful indication that a secosteroid of the vitamin D type was injected into the system.<sup>31</sup> The position of the hydroxyl group at the target C<sub>25</sub> position was established by the MS of the TMS derivative. The spectrum shows a prominent ion from the C<sub>24</sub>-C<sub>25</sub> bond cleavage, with characteristic fragment at *m/z* 131 and molecular ion at *m/z* 544. Additionally, characteristic fragments at *m/z* 529 ([M-15]<sup>+</sup>), *m/z* 454 ([M-90]<sup>+</sup>), *m/z* 439 ([M-90-15]<sup>+</sup>), *m/z* 349 ([M-90-90-15]<sup>+</sup>) and *m/z* 413 were also present. Therefore, both the chromatographic profiles and the mass spectra correspond to the isomerized secosteroids.

### Peroxygenase structure

A superimposition of the general structure and the haem pocket residues in *A. aegerita* and *C. cinerea* peroxygenases is shown in Fig. 3. The main differences are the two longer loops (Fig. 3A, arrows) and the substitution of Phe69 by Met69 (Fig. 3B, red label) in the *C. cinerea* enzyme. All other haem pocket residues, including the proximal cysteine acting

as the fifth ligand of the haem iron (Cys36) and the distal glutamic acid and arginine involved in haem activation by H<sub>2</sub>O<sub>2</sub> (Glu169 and Arg189),<sup>34</sup> are conserved in the two enzymes. Moreover, differences in the channel providing access to the haem cofactor and the neighbor residues at the channel entrance are shown in Fig. 4.

### Computational modeling

**Ligand diffusion energy profiles.** For the simulations of cholecalciferol and ergocalciferol access to the H<sub>2</sub>O<sub>2</sub>-activated haem in the *A. aegerita* and *C. cinerea* peroxygenases, the haem cofactor was modeled as compound I (an Fe<sup>IV</sup>=O porphyrin cation radical complex). The substrate was placed close to the entrance of the haem-access channel of the proteins prepared at the optimal pH for peroxygenase activity (pH 7). This initial location was identified using SiteMap,<sup>39</sup> and from there, the ligand was spawned inside the protein by PELE,<sup>10</sup> following the distance between the reactive O atom in the haem compound I and the cholecalciferol/ergocalciferol's C<sub>25</sub> atom (Fig. 1).

PELE simulations were done in two stages: first, the substrate is perturbed to reduce the C<sub>25</sub>-O distance and, when this distance is below 5 Å, the substrate is free to explore the active site cavity (at the haem distal side) with a 15 Å restrain. In the first step, the ligand is perturbed with a combination of large and small translations and rotations, ranging from 0.5 to 1.5 Å for translations, and 0.05 to 0.25 radians for rotations. However, during the second stage, the translation range is reduced (0.75–0.25 Å) to perform a finer active site exploration. The plots shown in Fig. 5 correspond to three 48 h simulations, each with 80 processors, and show the substrate-C<sub>25</sub> to haem-O distance vs. the interaction energy between the protein and the substrate at each of the different poses explored.

Simulations show that for the *A. aegerita* peroxygenase, the entrance of the substrates from the surface of the protein is quite favorable but then, the access to the activated haem is obtained against an uphill potential (Fig. 5A and B). For the *C. cinerea* enzyme, the entrance is less open than in the

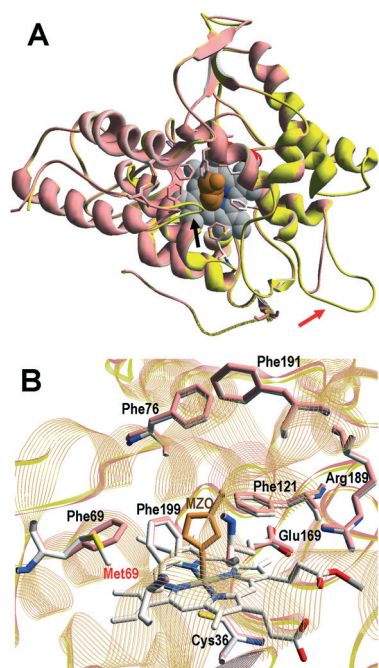


**Fig. 3** Comparison of peroxygenase molecular structures. A) General superimposition with the *A. aegerita* and *C. cinerea* proteins as pink and yellow ribbons, respectively. The haem group (CPK-colored spheres) and several haem pocket residues (pink- and CPK-colored sticks, respectively) are shown, and two larger loops in the second enzyme are indicated by arrows. B) Haem pocket residues in the *A. aegerita* (pink sticks) and *C. cinerea* (CPK-colored sticks) peroxygenases (red label indicates non-conserved methionine in position 69 of the latter enzyme). A hypothetical product molecule identified as 4-hydroxymethylimidazole is shown in A (brown-colored vdW spheres) and B (MZO, brown-colored sticks).<sup>34</sup> From *A. aegerita* PDB 2YOR, and *C. cinerea* homology model (provided in the ESI†).

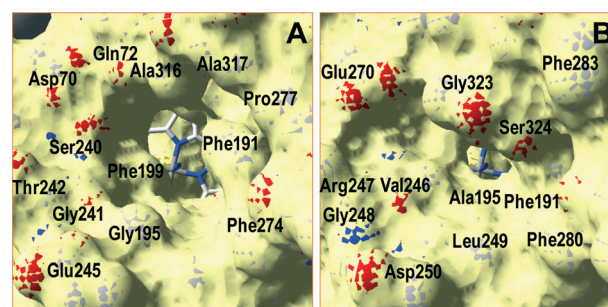


**Fig. 4** Solvent access surfaces showing differences in the size of the haem (CPK-colored sticks) access channel in the peroxygenases of *A. aegerita* (A) and *C. cinerea* (B). Several neighbor residues are shown as CPK-colored vdW spheres, including Gly323 and Ser324 contributing to occlude the haem channel in the *C. cinerea* enzyme.

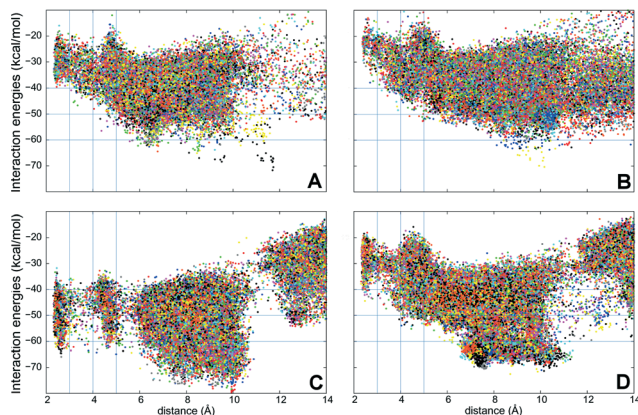


**Fig. 5** Interaction energies vs. ligand distances from PELE simulations for cholecalciferol (left) and ergocalciferol (right) entrance by the C<sub>25</sub> end in the peroxygenases from *A. aegerita* (A, B) and *C. cinerea* (C, D). The distances shown (Å) are between the reactive O atom in the haem compound I and the calciferol C<sub>25</sub> (for substrate numbering see Fig. 1).

*A. aegerita* peroxygenase and, for this reason, we observed a constrained access to the protein (at around 12 Å). However, the overall energy profile is more favorable, in particular for cholecalciferol (Fig. 5C). Once inside the protein, the ligand must surpass smaller barriers to reach the haem. From Fig. 5, it is clearly seen that *C. cinerea* peroxygenase has the most favorable energy profiles and well-defined minima in the active site (with C<sub>25</sub>–O distance around 3 Å). Fig. 5A and C show that the binding of cholecalciferol at the haem site is more favorable in the *C. cinerea* peroxygenase (–65 kcal mol<sup>–1</sup>) than in the *A. aegerita* enzyme (–40 kcal mol<sup>–1</sup>). This difference comes from the fact that the first protein has a tighter binding pocket (see below). In the case of ergocalciferol in Fig. 5B and D, the binding is also more favorable in the *C. cinerea* (–42 kcal mol<sup>–1</sup>) than in the *A. aegerita* enzyme (–30 kcal mol<sup>–1</sup>). These differences in the energy profiles, which indicate a more favorable protein–ligand interaction in *C. cinerea*, can explain the higher conversion rates observed for the two compounds in this peroxygenase.

**Ligand binding.** If we overlap cholecalciferol's positions for the entire PELE simulations for both proteins, we find two main orientations in the active site, as shown in Fig. 6.

The two orientations in Fig. 6B correspond to the two minima observed in cholecalciferol's diffusion in the *C. cinerea* peroxygenase (Fig. 5C). One of the minima (in green) is found at the binding distance to the haem O, and a second (in blue), about 5 Å away from the haem oxygen (Fig. 5C). The ligand's position observed in the *C. cinerea* peroxygenase is also found in the *A. aegerita* enzyme (Fig. 6A), although they do not correspond to the energy minima (Fig. 5A). Likewise, ergocalciferol can adopt two main positions in the binding pocket, although the minima (Fig. 5D) are less marked than that found for cholecalciferol (Fig. 5C).

When cholecalciferol is in an optimal reacting position, it is held in place by *C. cinerea*/*A. aegerita* peroxygenase

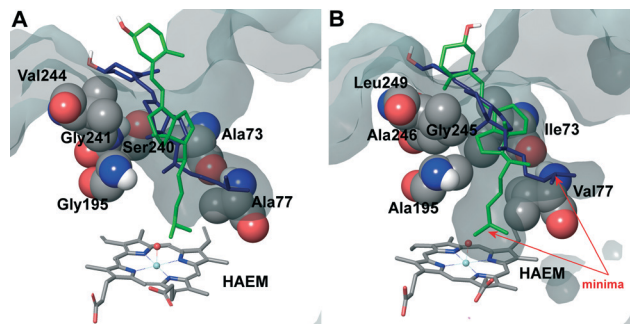


**Fig. 6** Superposition of cholecalciferol main active site positions (as liquorice) obtained in PELE simulations on the *A. aegerita* (A) and *C. cinerea* (B) peroxygenases. Haem cofactor also in liquorice and selected residues as vdW spheres. The protein's active site access is shown as a surface.

Val77/Ala77, Phe121/Phe121, Thr192/Thre192, Ala195/Gly195, Phe199/Phe199 and Glu196/Glu196 (Fig. S1†). It is worthy to note that Phe69 also contributes to substrate positioning in *A. aegerita* peroxygenase, but the homologous Met69 of the *C. cinerea* enzyme (Fig. 3B) is placed away from cholecalciferol and does not appear to have any effect on its position in the active site. Ergocalciferol, however, with an extra methyl group in position C<sub>24</sub> and with a C<sub>22</sub>–C<sub>23</sub> double bond (Fig. 1), is positioned in a slightly different manner in the active site, and residues in position 69 (phenylalanine and methionine) now interacts with the ligand (red arrows in Fig. S2†). This extra constraint could be responsible for the lower reactivity observed for D<sub>2</sub> in both peroxygenases. The influence of the side-chain structure (alkyl substituent and unsaturation presence) on the activity of the *A. aegerita* and *C. cinerea* peroxygenases was evidenced in the reaction of these enzymes with different sterols (Table S1†).

Inspection of the haem entrance when both ligands are in the active site reveals a better wrapping of the protein around the ligands in *C. cinerea* peroxygenase, compared with the *A. aegerita* enzyme. This is mainly due to the larger loop where Gly323 is located, which is smaller in the *A. aegerita* peroxygenase (Fig. 3A, black arrow). These are better illustrated in the haem-access channels of both peroxygenases in Fig. 4, where the position of the above Gly323 is shown. The narrower access to the haem in *C. cinerea* is also the result of several hydrophobic amino acid substitutions. Replacements to larger side chains in *C. cinerea* are dominant with: Ala73/Ile73, Ala77/Val77, Gly195/Ala195, Gly241/Ala246 and Val244/Leu249; and only one to a smaller amino acid, Ser240/Gly245. Due to the larger entrance cavity of the *A. aegerita* peroxygenase, both substrates remained solvent exposed at the C<sub>2</sub> end. In contrast, more favorable interactions are established at the final substrate position inside the tighter channel of the *C. cinerea* peroxygenase, which presents extra interactions on the protein surface. The combination of the surface interactions, along with a tighter haem cavity, result in the improved interaction energies seen for D<sub>2</sub> and D<sub>3</sub> in this protein.

**Site selectivity.** To investigate the different site selectivities observed for D<sub>2</sub> and D<sub>3</sub> hydroxylation by *A. aegerita* and *C. cinerea* peroxygenases, we have analysed the relative distance distribution of the substrates' reactive hydrogen atoms in the active site. We have considered as reactive those that can approach the haem compound I oxygen atom close enough to react. Thus, we have taken into account the hydrogen atoms in positions C<sub>24</sub>, C<sub>25</sub>, C<sub>26</sub> and C<sub>27</sub> for both ligands, in addition to C<sub>28</sub> hydrogen atoms for ergocalciferol. We have selected all structures (from the PELE simulations) where the distance between H–O is below 5 Å and interaction energies below  $-20 \text{ kcal mol}^{-1}$  for D<sub>2</sub> and  $-30 \text{ kcal mol}^{-1}$  for D<sub>3</sub>. When the relative frequency of these distances was computed (Fig. 7), it can be seen that for *C. cinerea*, the O–H<sub>25</sub> frequency is dominant for both compounds. Similar conclusions were obtained for both enzymes and substrates when the distribution of angles of Fe=O–H<sup>36</sup> was computed for the different reactive positions in the cholecalciferol and ergocalciferol side-chains (Fig. S3†).

The percentage of O–H<sub>25</sub> distances below 3 Å in *C. cinerea* is 54.5% for D<sub>3</sub> and 36.2% for D<sub>2</sub>, whereas in *A. aegerita* it is 27.4% and 25.7%, respectively. Moreover, in the D<sub>3</sub> simulations in *A. aegerita*, the fraction of structures with O–H<sub>24</sub> below 3 Å is 19.3%, which is quite high when compared to the other cases. In fact, the fraction of O–H<sub>25</sub> distances is

only 1.4 times superior to O–H<sub>24</sub> while for the other systems, it ranges between 10 to 20 times. This higher fraction of reactive O–H<sub>24</sub> distances can explain the observed formation of C<sub>24</sub> hydroxylated products in cholecalciferol. To sum up, and in agreement with experimental results, from the relative frequencies in *C. cinerea* peroxygenase, and also for ergocalciferol in *A. aegerita*, we expect a completely regio-selective reaction in C<sub>25</sub>. In contrast, for cholecalciferol in *A. aegerita* enzyme, it seems that hydroxyl addition is possible not only in C<sub>25</sub> position, but also in other carbons (C<sub>24</sub> and C<sub>26</sub>/C<sub>27</sub>).

## Conclusions

Atomic level simulations have been used here to rationalize the differences observed for ergocalciferol and cholecalciferol's conversion rates and site selectivity in two peroxygenases. The overall improved energy profiles in *C. cinerea*, the presence of favorable minima, and a high fraction of favorable O–H<sub>25</sub> distances agrees well with experimentally higher conversion rates.

The main structural differences between the *A. aegerita* and *C. cinerea* peroxygenases that modify the access of cholecalciferol to the activated haem are the changes Ala73/Ile73, Ala77/Val77, Gly195/Ala195, Gly241/Ala246 and Val244/

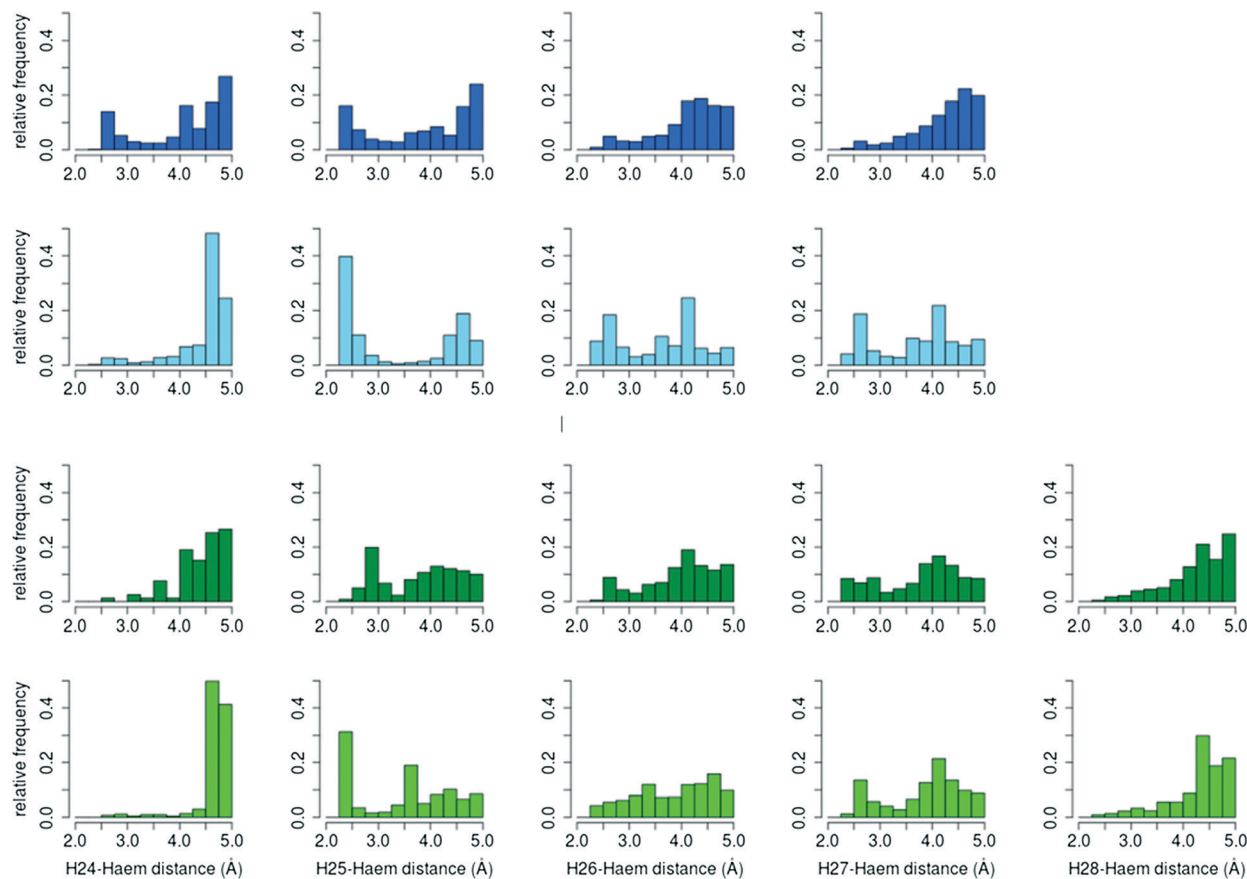


Fig. 7 Relative distance distributions of cholecalciferol (blue) and ergocalciferol (green) reactive hydrogen atoms to haem compound I oxygen atom. Histograms for *A. aegerita* are in dark colours, and in light colours for *C. cinerea*.

Leu249, all to larger amino acids, with only Ser240/Gly245 to a smaller one. These larger hydrophobic side chains augment the interaction of D<sub>2</sub> and D<sub>3</sub> substrates with *C. cinerea*. The better conversion rates observed for *C. cinerea* peroxygenase do not originate in the active site itself (where Phe69 is replaced by Met69), but in the ligand access to the active site instead, especially in the entrance to the protein. In particular, the larger loop hosting Gly323 creates a barrier that reduces the size of the entrance channel in the *C. cinerea* peroxygenase. This, along with a tighter cavity, is reflected in the more favorable interaction energies.

Although the improved reactivity of *C. cinerea* does not appear to be affected by the larger Phe69 side chain, it does hinder the entrance of ergocalciferol relative to cholecalciferol. The presence of an extra methyl group that interacts directly with position 69 in both proteins lowers the reactivity of this compound. Finally, the computed relative frequency of the distances between the activated haem oxygen and the hydrogen atoms in C<sub>24</sub> and C<sub>25</sub> show that, despite the more favourable hydroxylation on tertiary carbons, the reaction at cholecalciferol C<sub>24</sub> occurs when the ratio of favourable O–H<sub>25</sub>/O–H<sub>24</sub> distances decreases.

## Materials and methods

### Enzymes and chemicals

Peroxygenase (isoform II) was isolated from *A. aegerita* DSM 22459 grown in soybean medium using a combination of SP-Sephadex chromatography and Mono-P chromatofocusing.<sup>45</sup> *A. aegerita* DSM 22459 is deposited at the *Deutsche Stammsammlung für Mikroorganismen und Zellkulturen* Braunschweig (Germany). *C. cinerea* peroxygenase was provided by Novozymes A/S (Bagsvaerd, Denmark). The enzyme corresponds to the protein model 7249 from the sequenced *C. cinerea* genome available at the JGI (<http://genome.jgi.doe.gov/Copci1>), which was expressed in *Aspergillus oryzae* and purified using a combination of S-Sephadex and SP-Sephadex ion-exchange chromatography (patent WO/2008/119780). One peroxygenase unit is defined as the amount of enzyme oxidizing 1 μmol of veratryl alcohol to veratraldehyde ( $\epsilon_{310}$  9300 M<sup>-1</sup> cm<sup>-1</sup>) in 1 min at 24 °C, pH 7, after addition of 0.5 mM H<sub>2</sub>O<sub>2</sub> in the *C. cinerea* peroxygenase reactions and 2.5 mM H<sub>2</sub>O<sub>2</sub> in those with the *A. aegerita* peroxygenase.

Vitamin D<sub>3</sub>, also known as calciol or cholecalciferol ((5Z,7E)-(3S)-9,10-seco-5,7,10(19)-cholestatrien-3-ol; Fig. 1, structure 1), was tested as substrate of the *A. aegerita* and *C. cinerea* peroxygenases. 25-Hydroxyvitamin D<sub>3</sub>, also known as caldidiol or 25-hydroxycholecalciferol ((5Z,7E)-(3S)-9,10-seco-5,7,10(19)-cholestatriene-3,25-diol; Fig. 1 structure 2), was used as standard for gas chromatography-mass spectrometry (GC-MS) analyses. Vitamin D<sub>2</sub>, also known as ercalciol or ergocalciferol ((5Z,7E,22E)-(3S)-9,10-seco-5,7,10(19),22-ergostatetraen-3-ol; Fig. 1, structure 3), was also tested as substrate of the two peroxygenases. 25-Hydroxyvitamin D<sub>2</sub>, also known as ercaldidiol or 25-hydroxyergocalciferol ((5Z,7E,22E)-(3S)-9,10-seco-5,7,10(19),22-ergostatetraene-3,25-diol; Fig. 1,

structure 4), was also used as standard for GC-MS analyses. All compounds were from Sigma-Aldrich.

### Enzymatic reactions

Reactions of cholecalciferol and ergocalciferol (0.1 and 0.5 mM) with the *A. aegerita* and *C. cinerea* peroxygenases (1 U) were performed in 5 mL of 50 mM sodium phosphate, pH 7, at 40 °C for 60 min, in the presence of 0.5 mM H<sub>2</sub>O<sub>2</sub>. The substrates were previously dissolved in acetone, and added to the buffer (the acetone concentration in the reaction was 40%). In control experiments, the substrates were treated under the same conditions (including H<sub>2</sub>O<sub>2</sub>) but without enzyme. After the enzymatic reactions, the products were recovered by liquid-liquid extraction with methyl *tert*-butyl ether, dried under N<sub>2</sub>, and redissolved in chloroform for GC-MS analyses. Bis(trimethylsilyl)trifluoroacetamide (Supelco) in the presence of pyridine was used to prepare trimethylsilyl (TMS) derivatives. An internal standard was added after the enzymatic reactions to determine product yields.

### GC-MS analyses

GC-MS analyses were performed with a Shimadzu QP2010 Ultra equipment, using a fused-silica DB-5HT capillary column (30 m × 0.25 mm internal diameter, 0.1 μm film thickness) from J&W Scientific.<sup>16</sup> The oven was heated from 120 °C (1 min) to 300 °C (15 min) at 5 °C min<sup>-1</sup>. The injection was performed at 300 °C, the transfer line was kept at 300 °C, and helium was used as carrier gas. Compounds were identified by mass fragmentography and by comparing their mass spectra with standards, and quantitation was obtained from total-ion peak area using molar response factors obtained from cholecalciferol, ergocalciferol, 25-hydroxycholecalciferol and 25-hydroxyergocalciferol standards. The two latter compounds were also used as external standards for calculation of product yields.

### PELE and other computational analyses

The starting structures for PELE simulations were the *A. aegerita* peroxygenase crystal (2YOR)<sup>34</sup> and a homology model for the *C. cinerea* peroxygenase structure obtained using 2YOR as the template.<sup>8</sup> As the optimum pH for peroxygenase activity is 7, the structures were prepared accordingly using Schrodinger's Protein Preparation Wizard<sup>35</sup> and H++ web server.<sup>1</sup> Histidines were δ-protonated, with the exception of His82 (ε-protonated) and His118 and His251 (double protonated). All acidic residues were deprotonated, except for Asp85 which was kept in its protonated state. The ergocalciferol and cholecalciferol molecules were optimized with Jaguar<sup>37</sup> at the DFT/M06 level with the 6-31G\*\* basis and a PBF implicit solvent in order to obtain their electrostatic potential atomic charges. Finally, the haem site was modeled as thiolate-ligated compound I after being fully optimized in the protein environment with quantum mechanics/molecular mechanics (QM/MM) using QSite.<sup>38</sup> The electronic calculations show three unpaired electrons: two located on the oxoiron group

and a third on the heme and less than 1% spin contamination.

Once the initial protein structure was prepared and ligands optimized, these were placed manually in identical positions at the entrance of the haem-access channel and PELE simulations were performed.<sup>10</sup> PELE is a Monte Carlo-based algorithm that produces new configurations through a sequential ligand and protein perturbation, side chain prediction and minimization steps, freely available at <https://pele.bsc.es>. New configurations are then filtered with a Metropolis acceptance test, where the energy is described with an all-atom OPLS force field<sup>22</sup> and a surface generalized Born solvent.<sup>7</sup> In this way, it is possible to locate and characterize local and global minima structures for the most favorable protein–ligand interactions. PELE has been successfully used in a number of ligand migration studies with both small and large substrates.<sup>18,29,30</sup>

Distance and angle distributions were computed after screening all structures from PELE simulations by using the interaction energy and distance to the compound I oxygen atom. The structures which showed interaction energies below  $-20 \text{ kcal mol}^{-1}$  for ergocalciferol and  $-30 \text{ kcal mol}^{-1}$  for cholecalciferol were selected. Reactive hydrogen atoms were considered to be below  $5 \text{ \AA}$  from the compound I oxygen atom for the distance analysis and  $3 \text{ \AA}$  for the angle study (angles are much more sensitive and thus only near attack conformations were selected). All the selected structures were then used to compute the relative frequencies of the ligand's hydrogen atoms at reactive distances to the haem oxygen and Fe=O–H and O–H–C angles.

## Acknowledgements

This work was supported by the INDOX (KBBE-2013-7-613549) and PELE (ERC-2009-Adg 25027) EU projects, and by the BIO2011-26694 and CTQ2013-48287 projects of the Spanish Ministry of Economy and Competitiveness.

## Notes and references

- R. Anandakrishnan, B. Aguilar and A. V. Onufriev, *Nucleic Acids Res.*, 2012, **40**, W537–W541.
- E. Aranda, M. Kinne, M. Kluge, R. Ullrich and M. Hofrichter, *Appl. Microbiol. Biotechnol.*, 2009, **82**, 1057–1066.
- E. Aranda, R. Ullrich and M. Hofrichter, *Biodegradation*, 2010, **21**, 267–281.
- E. D. Babot, J. C. del Río, M. Cañellas, F. Sancho, F. Lucas, V. Guallar, L. Kalum, H. Lund, G. Gröbe, K. Scheibner, R. Ullrich, M. Hofrichter, A. T. Martínez and A. Gutiérrez, *Appl. Environ. Microbiol.*, 2015, **81**, 4130–4142.
- E. D. Babot, J. C. del Río, L. Kalum, A. T. Martínez and A. Gutiérrez, *Biotechnol. Bioeng.*, 2013, **110**, 2332.
- E. D. Babot, J. C. del Río, L. Kalum, A. T. Martínez and A. Gutiérrez, *ChemCatChem*, 2015, **7**, 283–290.
- D. Bashford and D. A. Case, *Annu. Rev. Phys. Chem.*, 2000, **51**, 129–152.
- L. Bordoli, F. Kiefer, K. Arnold, P. Benkert, J. Battey and T. Schwede, *Nat. Protoc.*, 2009, **4**, 1–13.
- S. Bormann, A. G. Baraibar, Y. Ni, D. Holtmann and F. Hollmann, *Catal. Sci. Technol.*, 2015, **5**, 2038–2052.
- K. W. Borrelli, A. Vitalis, R. Alcantara and V. Guallar, *J. Chem. Theory Comput.*, 2005, **1**, 1304–1311.
- N. R. Buck, W. Claerhout, B. H. Leuenberger, E. Stoecklin, K. Urban and S. Wolfram, *US Pat.*, US20130210782 A1, 2013.
- B. P. Cossins, A. Hosseini and V. Guallar, *J. Chem. Theory Comput.*, 2012, **8**, 959–965.
- D. Floudas, M. Binder, R. Riley, K. Barry, R. A. Blanchette, B. Henrissat, A. T. Martínez, R. Otilar, J. W. Spatafora, J. S. Yadav, A. Aerts, I. Benoit, A. Boyd, A. Carlson, A. Copeland, P. M. Coutinho, R. P. de Vries, P. Ferreira, K. Findley, B. Foster, J. Gaskell, D. Glotzer, P. Górecki, J. Heitman, C. Hesse, C. Hori, K. Igarashi, J. A. Jurgens, N. Kallen, P. Kersten, A. Kohler, U. Kües, T. K. A. Kumar, A. Kuo, K. LaButti, L. F. Larrondo, E. Lindquist, A. Ling, V. Lombard, S. Lucas, T. Lundell, R. Martin, D. J. McLaughlin, I. Morgenstern, E. Morin, C. Murat, M. Nolan, R. A. Ohm, A. Patyshakuliyeva, A. Rokas, F. J. Ruiz-Dueñas, G. Sabat, A. Salamov, M. Samejima, J. Schmutz, J. C. Slot, F. StJohn, J. Stenlid, H. Sun, S. Sun, K. Syed, A. Tsang, A. Wiebenga, D. Young, A. Pisabarro, D. C. Eastwood, F. Martin, D. Cullen, I. V. Grigoriev and D. S. Hibbett, *Science*, 2012, **336**, 1715–1719.
- C. A. Fritts and P. W. Waldroup, *J. Appl. Poult. Res.*, 2003, **12**, 45–52.
- A. Gutiérrez, E. D. Babot, R. Ullrich, M. Hofrichter, A. T. Martínez and J. C. del Río, *Arch. Biochem. Biophys.*, 2011, **514**, 33–43.
- A. Gutiérrez, J. C. del Río, F. J. González-Vila and F. Martín, *J. Chromatogr.*, 1998, **823**, 449–455.
- J. M. Hernández, *US Pat.*, US20130137662 A1, 2013.
- A. Hernández-Ortega, F. Lucas, P. Ferreira, M. Medina, V. Guallar and A. T. Martínez, *J. Biol. Chem.*, 2011, **286**, 41105–41114.
- M. Hofrichter and R. Ullrich, *Curr. Opin. Chem. Biol.*, 2014, **19**, 116–125.
- G. Jean, J. C. Terrat, T. Vanel, J. M. Hurot, C. Lorriaux, B. Mayor and C. Chazot, *Nephrol., Dial., Transplant.*, 2008, **23**, 3670–3676.
- G. Jones, *Annu. Rev. Nutr.*, 2013, **33**, 23–44.
- G. A. Kaminski, R. A. Friesner, J. Tirado-Rives and W. L. Jorgensen, *J. Phys. Chem. B*, 2001, **105**, 6474–6487.
- S. Käppeli, E. Frohlich, S. G. Gebhardt-Henrich, A. Pfulg, H. Schäublin, R. Zweifel, H. Wiedmer and H. H. Stoffel, *Arch. Geflügelkd.*, 2011, **75**, 179–184.
- A. Karich, M. Kluge, R. Ullrich and M. Hofrichter, *AMB Express*, 2013, **3**, 5.
- M. Kinne, C. Zeisig, R. Ullrich, G. Kayser, K. E. Hammel and M. Hofrichter, *Biochem. Biophys. Res. Commun.*, 2010, **397**, 18–21.
- M. Kluge, R. Ullrich, C. Dolge, K. Scheibner and M. Hofrichter, *Appl. Microbiol. Biotechnol.*, 2009, **81**, 1071–1076.

- 27 M. Kluge, R. Ullrich, K. Scheibner and M. Hofrichter, *Green Chem.*, 2012, **14**, 440–446.
- 28 G. A. Leichtmann, J. M. Bengoa, M. J. G. Bolt and M. D. Sitrin, *Am. J. Clin. Nutr.*, 1991, **54**, 548–552.
- 29 D. Linde, R. Pogni, M. Cañellas, F. Lucas, V. Guallar, M. C. Baratto, A. Sinicropi, V. Sáez-Jiménez, C. Coscolín, A. Romero, F. J. Medrano, F. J. Ruiz-Dueñas and A. T. Martínez, *Biochem. J.*, 2015, **466**, 253–262.
- 30 M. F. Lucas and V. Guallar, *Biophys. J.*, 2012, **102**, 887–896.
- 31 H. L. J. Makin and D. B. Gower, *Steroid analysis*, Springer, NY, 2010.
- 32 M. Michalczyk, D. Pietrzak, J. Niemiec and J. Mroczk, *Pol. J. Food Nutr. Sci.*, 2010, **60**, 121–126.
- 33 S. Peter, M. Kinne, X. Wang, R. Ulrich, G. Kayser, J. T. Groves and M. Hofrichter, *FEBS J.*, 2011, **278**, 3667–3675.
- 34 K. Piontek, E. Strittmatter, R. Ullrich, G. Grobe, M. J. Pecyna, M. Kluge, K. Scheibner, M. Hofrichter and D. A. Plattner, *J. Biol. Chem.*, 2013, **288**, 34767–34776.
- 35 G. M. Sastry, M. Adzhigirey, T. Day, R. Annabhimoju and W. Sherman, *J. Comput.-Aided Mol. Des.*, 2013, **27**, 221–234.
- 36 J. C. Schöneboom, S. Cohen, H. Lin, S. Shaik and W. Thiel, *J. Am. Chem. Soc.*, 2004, **126**, 4017–4034.
- 37 *Schrödinger. Jaguar 7.8*, LCC, New York, 2011.
- 38 *Schrödinger. QSite 5.7*, LCC, New York, 2011.
- 39 *Schrödinger. SiteMap 2.5*, LCC, New York, 2011.
- 40 C. Simoes-Nunes and G. M. Weber, *EP Pat.*, EP1516540 B1, 2004.
- 41 M. D. Sitrin and J. M. Bengoa, *Am. J. Clin. Nutr.*, 1987, **46**, 1011–1015.
- 42 R. Ullrich, C. Dolge, M. Kluge and M. Hofrichter, *FEBS Lett.*, 2008, **582**, 4100–4106.
- 43 R. Ullrich and M. Hofrichter, *FEBS Lett.*, 2005, **579**, 6247–6250.
- 44 R. Ullrich and M. Hofrichter, *Cell. Mol. Life Sci.*, 2007, **64**, 271–293.
- 45 R. Ullrich, J. Nuske, K. Scheibner, J. Spantzel and M. Hofrichter, *Appl. Environ. Microbiol.*, 2004, **70**, 4575–4581.

## Supporting Information

### Molecular determinants for selective C<sub>25</sub>-hydroxylation of vitamins D<sub>2</sub> and D<sub>3</sub> by fungal peroxygenases

Fátima Lucas,<sup>1,a\*</sup> Esteban D. Babot,<sup>1,b</sup> Marina Cañellas,<sup>1,a,c</sup> José C. del Río,<sup>b</sup> Lisbeth Kalum,<sup>d</sup> René Ullrich,<sup>e</sup> Martin Hofrichter,<sup>e</sup> Victor Guallar,<sup>a,f</sup> Angel T. Martínez<sup>g</sup> and Ana Gutiérrez<sup>b\*</sup>

<sup>1</sup> These three authors equally contributed to this work

<sup>a</sup> Joint BSC-CRG-IRB Research Program in Computational Biology, Barcelona Supercomputing Center, Jordi Girona 29, E-08034 Barcelona, Spain, E-mail: fati.lucas@gmail.com

<sup>b</sup> Instituto de Recursos Naturales y Agrobiología de Sevilla, CSIC, Reina Mercedes 10, E-41012 Seville, Spain. E-mail: anagu@irnase.csic.es; Fax: +32 954624002; Tel: +32 954624711

<sup>c</sup> Anaxomics Biotech, Balmes 89, E-08008 Barcelona, Spain

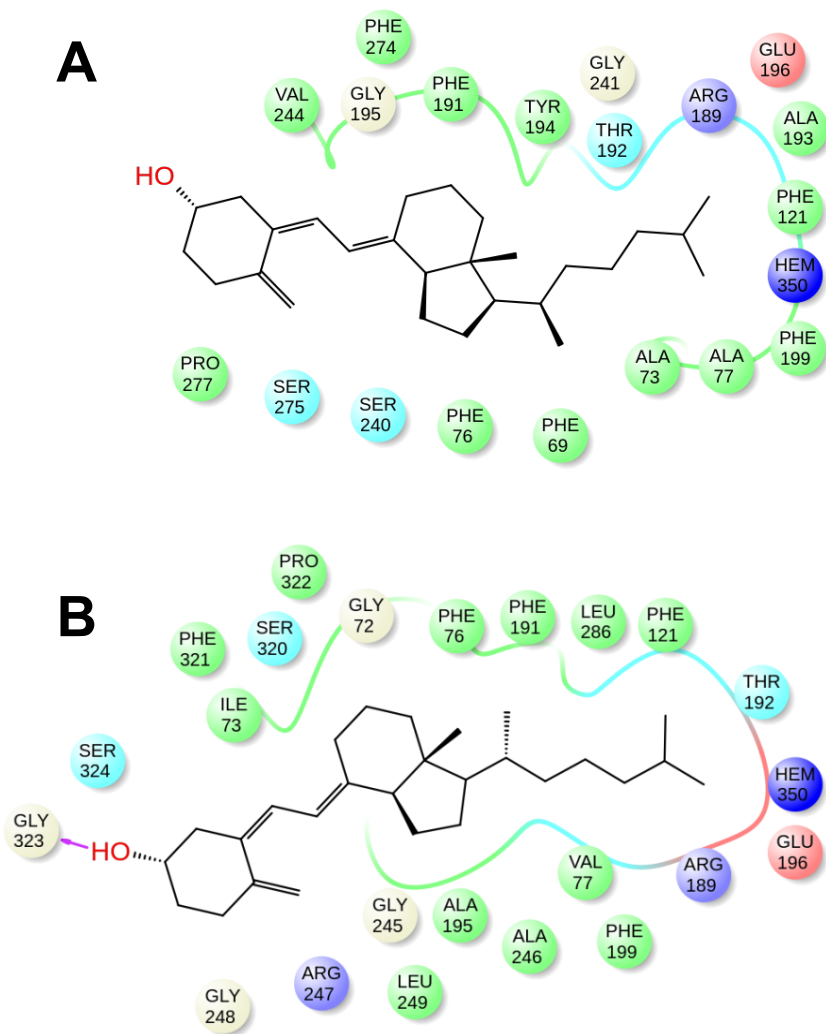
<sup>d</sup> Novozymes A/S, Krogshøjvej 36, 2880 Bagsvaerd, Denmark

<sup>e</sup> TU Dresden, Department of Bio- and Environmental Sciences, Markt 23, 02763 Zittau, Germany

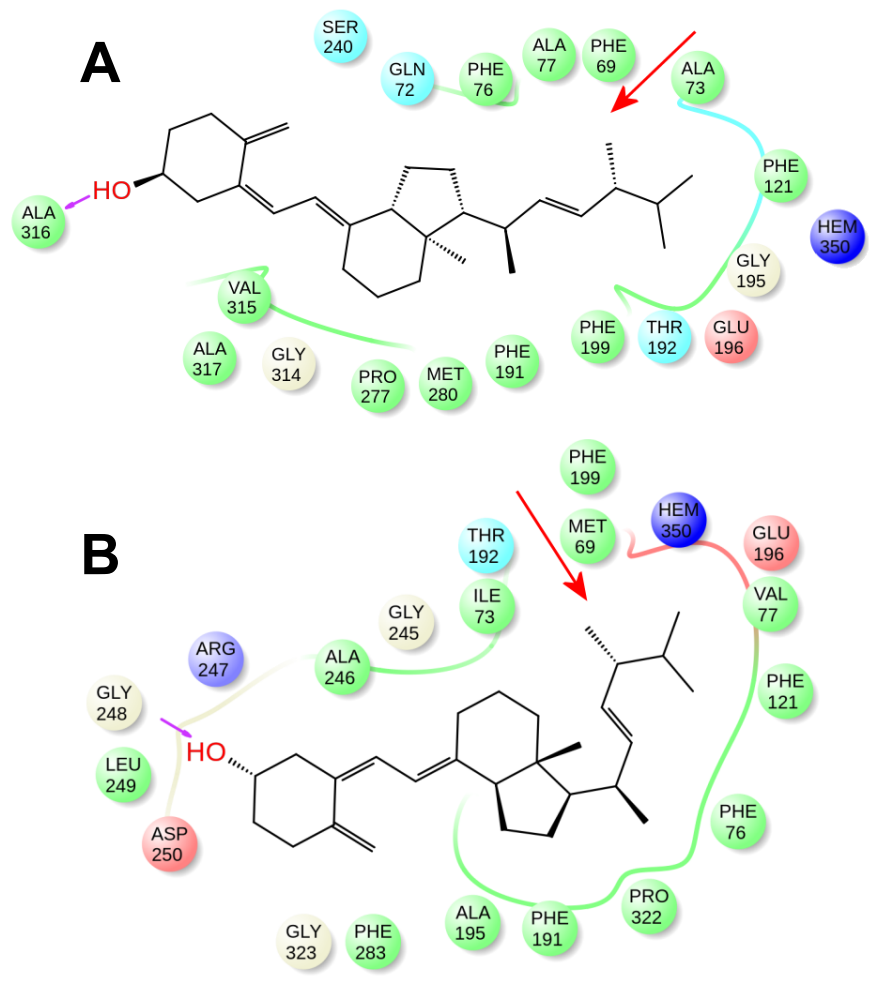
<sup>f</sup> ICREA, Passeig Lluís Companys 23, E-08010 Barcelona, Spain

<sup>g</sup> Centro de Investigaciones Biológicas, CSIC, Ramiro de Maeztu 9, E-28040 Madrid, Spain

The Supporting Information shows the main interactions of cholecalciferol and ergocalciferol at the peroxygenase heme access channel (**Fig. S1** and **S2**, respectively), the effect of side-chain structure on the conversion rates of five sterols by the *A. aegerita* and *C. cinerea* peroxygenases (**Table S1**), and distributions of estimated Fe=O-H and O-H-C angles in the peroxygenase reactions with cholecalciferol and ergocalciferol (**Fig. S3**).

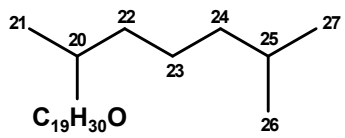
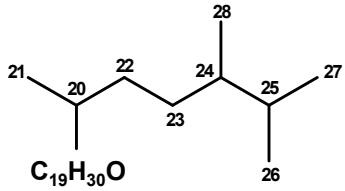
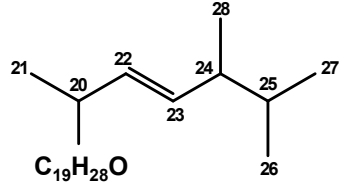
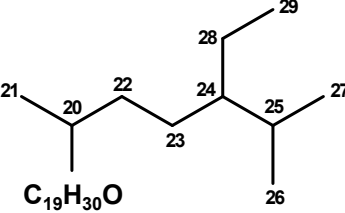
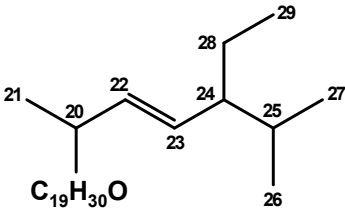


**Fig. S1** Main interactions (below 3 Å) for cholecalciferol with the peroxygenases of *A. aegerita* (**A**) and *C. cinerea* (**B**).



**Fig. S2** Main interactions (below 3 Å) for ergocalciferol with the peroxygenases of *A. aegerita* (A) and *C. cinerea* (B).

**Table S1** Conversion degree of steroids with different side-chains (A-E: cholesterol, campesterol, ergosterol, sitosterol and stigmasterol, respectively) by *A. aegerita* and *C. cinerea* peroxygenases<sup>a</sup>

	Conversion (%)	
	<i>A. aegerita</i> peroxygenase	<i>C. cinerea</i> peroxygenase
<p><b>A</b></p>  <p><b>C<sub>19</sub>H<sub>30</sub>O</b></p>	64	100
<p><b>B</b></p>  <p><b>C<sub>19</sub>H<sub>30</sub>O</b></p>	47	30
<p><b>C</b></p>  <p><b>C<sub>19</sub>H<sub>28</sub>O</b></p>	10	6
<p><b>D</b></p>  <p><b>C<sub>19</sub>H<sub>30</sub>O</b></p>	13	6
<p><b>E</b></p>  <p><b>C<sub>19</sub>H<sub>30</sub>O</b></p>	2	2

<sup>a</sup>From E. D. Babot, J. C. del Río, M. Cañellas, F. Sancho, F. Lucas, V. Guallar, L. Kalum, H. Lund, G. Gröbe, K. Scheibner, R. Ullrich, M. Hofrichter, A. T. Martínez, and A. Gutiérrez. 2015. Steroid hydroxylation by basidiomycete peroxygenases: A combined experimental and computational study. *Appl. Environ. Microbiol.* 81:4130-4142

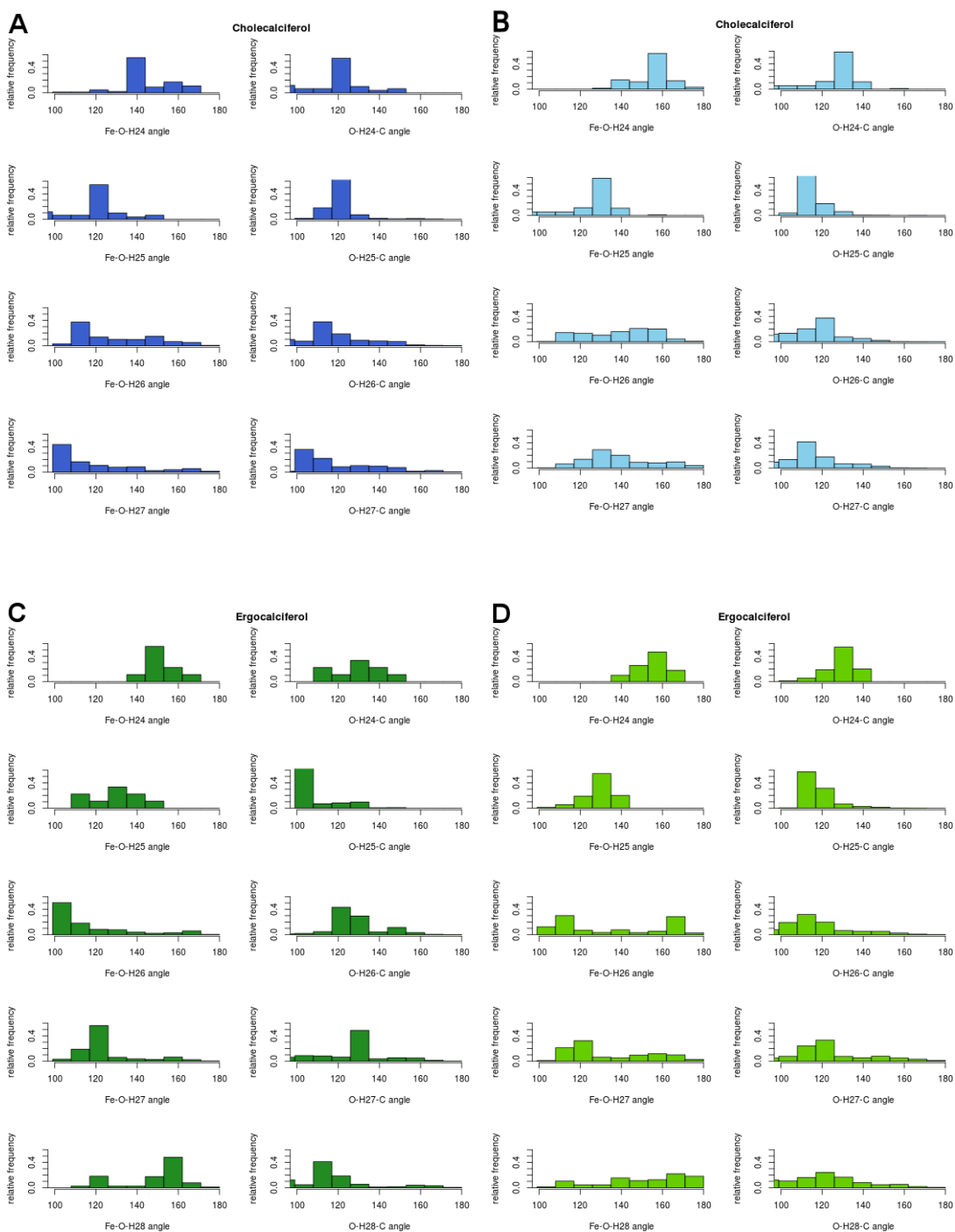


**Fig. S3** Relative distributions of computed Fe=O-H and O-H-C angles for the reactions of *A. aegerita* (**A, C**) and *C. cinerea* (**B, D**) peroxygenases at the C<sub>24</sub>, C<sub>25</sub>, C<sub>26</sub> and C<sub>27</sub>, positions of cholecalciferol (blue) and ergocalciferol (green) and the C<sub>28</sub> position of ergocalciferol. Structures were filtered by energy and distance between the pertinent hydrogen atom and the haem compound I oxygen (below 3 Å). QM/MM studies for P450<sub>cam</sub><sup>b</sup> show that in a pre-arranged reactive position camphor adopts angles of 130° for Fe=O-H and 170° for O-H-C. While for that latter no correlation is found to the theoretical predictions, in the case of Fe=O-H<sub>24</sub> angles between 120 and 140° are favoured in C<sub>24</sub> for cholecalciferol reacting with *A. aegerita* (**A**) in

agreement with the experimentally observed formation of 21% product in this position. In the case of the remaining 3 reactions, few structures are found with angles below  $145^\circ$ . In the case of Fe=O-H<sub>25</sub> (as expected) all compounds present favourable angles. Analogous to the case of the distance distribution analysis, no conclusions can be made for the reactivity of C<sub>26</sub>, C<sub>27</sub> and C<sub>28</sub>.

<sup>b</sup>J. C. Schöneboom, S. Cohen, H. Lin, S. Shaik and W. Thiel, *J. Am. Chem. Soc.*, 2004, 126, 4017-4034